

# Direct control of high magnetic fields for cold atom experiments based on NV centers

Alexander Hesse,<sup>1</sup> Kerim Köster,<sup>1</sup> Jakob Steiner,<sup>2,3</sup> Julia Michl,<sup>2</sup> Vadim Vorobyov,<sup>2</sup> Durga Dasari,<sup>2</sup> Jörg Wrachtrup,<sup>2,4</sup> and Fred Jendrzejewski<sup>1</sup>

<sup>1</sup>*Kirchhoff-Institut für Physik, Im Neuenheimer Feld 227, 69120 Heidelberg*  
<sup>2</sup>*3. Physikalisches Institut, Center for Applied Quantum Technologies, IQST, Pfaffenwaldring 57, 70569 Stuttgart*

<sup>3</sup>*Paul-Scherrer-Institute, 5323 Villigen, Switzerland*

<sup>4</sup>*Max Planck Institute for Solid State Research, Heisenbergstrae 1, 70569 Stuttgart, Germany*

(Dated: March 19, 2020)

In atomic physics experiments, magnetic fields allow to control the interactions between atoms, e.g. near Feshbach resonances, or by employing spin changing collisions. The magnetic field control is typically performed indirectly, by stabilizing the current of Helmholtz coils producing the large bias field. Here, we overcome the limitations of such an indirect control through a direct feedback scheme, which is based on nitrogen-vacancy centers acting as a sensor. This allows us to measure and stabilize magnetic fields of 46.6 G down to 1.2 mG RMS noise, with the potential of reaching much higher field strengths. Because the magnetic field is measured directly, we reach minimum shot-to-shot fluctuations of 0.32(4) ppm on a 22 minute time interval, ensuring high reproducibility of experiments. This approach extends the direct magnetic field control to high magnetic fields, which could enable new precise quantum simulations in this regime.

## I. INTRODUCTION

The direct control of modest magnetic fields up to 10 Gauss enabled experiments with cold atoms on spin squeezing close to a Feshbach resonance [1, 2], while tuning the fields directly to values below 1 mG made the controlled investigation of spontaneous demagnetization possible [3]. More recently it was employed for the quantum simulation of scaling dynamics far from equilibrium [4] and a scalable building block for lattice gauge theories in atomic mixtures [5].

In all these cases, the direct magnetic field control is based on active feedback from a fluxgate sensor, which limits this class of experiments to magnetic fields below 10 Gauss, the working range of fluxgate sensors [6]. Many phenomena, like droplet formation close to a heteronuclear Feshbach resonance [7], or spin changing collisions between fermionic and bosonic species [8], do however occur at much higher field strengths, reaching up to a few 100 Gauss. Direct magnetic field control has so far not been possible at these values due to a lack of high precision sensors, making precision experiments challenging.

This shows the need for alternative sensors, with the ability to measure large magnetic fields with high precision. Over the last years, several sensors based on quantum systems with the potential to close this gap have been tested: Most prominently, SQUIDs can measure magnetic fields with sensitivities below  $1 \text{ nG}/\sqrt{\text{Hz}}$  [9, 10], with atomic gases reaching only slightly worse sensitivities [11, 12]. However, these systems are fairly bulky and complicated to set up, making them impractical as a sensor for an active magnetic field stabilization.

The nitrogen-vacancy (NV) center in diamond provides a versatile and compact magnetic field sensor, covering ranges of several hundreds of Gauss with precisions below  $10 \text{ nG}/\sqrt{\text{Hz}}$  [13] for AC magnetic fields. For measurements which approach the DC regime, sensitivities of 500 nG have been reported [14]. Due to their small size, they

are the perfect candidate for magnetic field stabilizations past the range of fluxgate sensors, and allow the study of spin dynamics in regimes previously not experimentally accessible.

In this letter, we investigate the direct control of homogeneous magnetic fields based on such NV centers. Our experimental setup is sketched in Fig. 1. A set of Helmholtz coils produces a homogeneous magnetic field  $B_0$ , which is directly proportional to the applied control current flowing through the coils. The magnetic field is sensed through the fluorescence of a compact NV center magnetometer. In the magnetometer we measure the optically detected magnetic-resonance features (ODMR) by dressing the ground state spin triplet with a microwave signal of frequency  $\nu$ . A dip appears in the fluorescence intensity of the NV center  $I$  when one of the magnetic field projections onto the NV center orientations coincides with the Zeeman shifted transition frequency [15]. The derivative  $S = dI/d\nu$  is then used as an error signal for the feedback loop. The controlled field has been monitored through a second, independent NV magnetometer over the course of 24 hours. For two measurements, separated by 22 minutes fluctuations are minimal, reaching 0.32(4) ppm. In future applications, this second diamond magnetometer will be replaced by the cold atomic clouds of interest.

The remainder of the paper is structured as follows. In section II, we review the employed detection of the magnetic field and how we separate thermal drifts from magnetic field changes. In III we discuss the control of the magnetic field through the Helmholtz coils and finally benchmark our system in IV in a detailed fashion. We end with an outlook for even more compact solutions beyond this proof-of-concept.

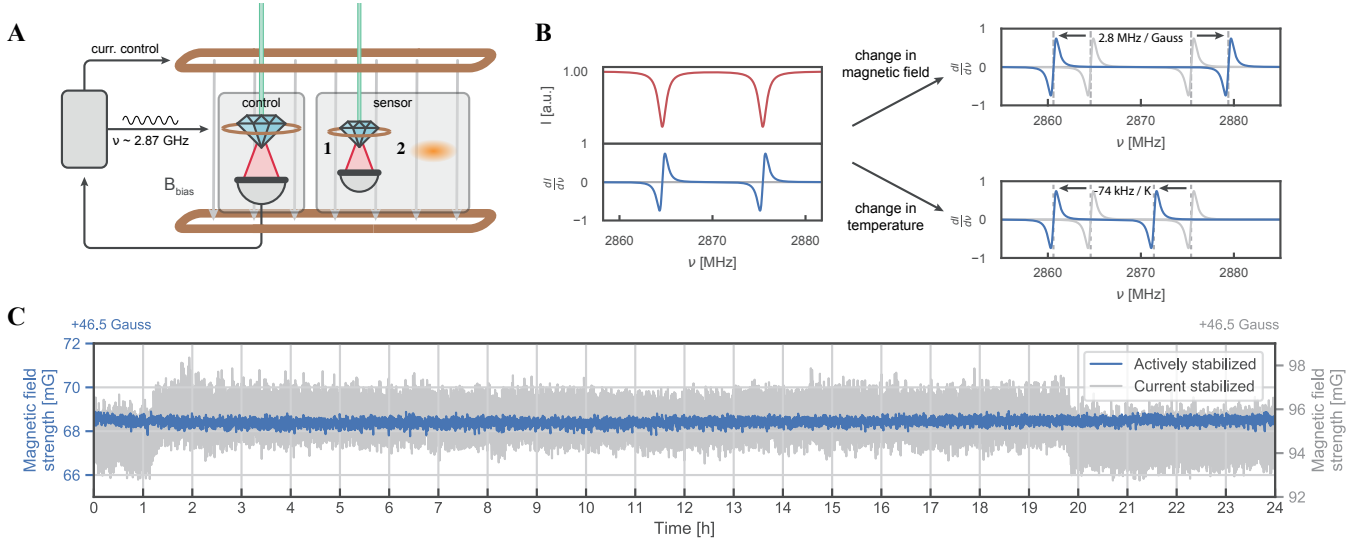


FIG. 1. (A) Basic experimental setup: The NV centers are positioned in a magnetic field generated by a pair of Helmholtz coils. They are excited by a green laser, and their red fluorescence is collected on a photodiode. This signal is fed into a control circuit, which also generates the microwave signal applied to the NV centers via a wire loop. From the fluorescence a magnetic field reading is extracted, and used to regulate the current through a second, low inductance coil pair. (1) The quality of the magnetic field stabilization is monitored on a second, independent setup placed close to the first sample. (2) In the future, this second NV sensor will be replaced by the cold quantum gas used in our experiments, such that it experiences stable magnetic fields. (B) Shift of the two transitions  $m_s = 0 \rightarrow m_s = -1$  and  $m_s = 0 \rightarrow m_s = 1$  with temperature and magnetic field, as visible in the fluorescence signal. Using a lock in scheme we extract the derivative of the spectrum. (C) Stabilized vs. unstabilized magnetic field, as seen on a second, independent sensor. In addition to higher noise for the unstabilized field, jumps in the field strength created by other experiments are visible.

## II. MAGNETOMETRY METHOD

For generating the magnetic field signal on both our sensors we employ an ODMR scheme [16], whose operation we summarize here. The NV center has a spin  $S = 1$  in its ground state, whose level structure is visualized in Fig. 2. It is optically pumped by a green laser, and emits strong fluorescence above 650 nm if the NV center is in the  $m_s = 0$  Zeeman level. The  $m_s = \pm 1$  states lie  $D \approx 2.87$  GHz (also called the zero field splitting (ZFS)) above the  $m_s = 0$  state and hence can be coupled to the ground state through standard microwave techniques. At nonzero magnetic field, the  $m_s = \pm 1$  states experience a Zeeman shift of approximately  $\pm \hbar \gamma_e \vec{B}_0 \hat{n}$ , where  $B_0$  is the magnetic field strength,  $\gamma_e = 2.8 \frac{\text{MHz}}{\text{Gauss}}$  is the gyromagnetic ratio of the electron, and  $\hat{n}$  is the projection of the magnetic field onto the NV center axis. For the  $m_s = \pm 1$  states, a nonradiative decay channel to the ground state leads to a slight decrease in fluorescence, allowing us to extract the transition frequencies  $\nu_{+1}$  and  $\nu_{-1}$  from the fluorescence spectrum (shown in Fig. 1 B).

## III. EXPERIMENTAL SETUP

The diamond samples used were grown with the HPHT technique, have a natural abundance of  $^{13}\text{C}$  and are type 1b diamonds. We place the sample in a homogeneous

magnetic field generated by a pair of rectangular coils (driven by a Delta Electronika SM 18-50) of side lengths  $33.5 \text{ cm} \times 28.5 \text{ cm}$  with 80 windings each and separated by 15.5 cm to ensure that both sensors experience the same magnetic field. A second pair of coils with 16 windings wound onto the first coil pair is used in combination with a homebuilt current driver to regulate the magnetic field with a high bandwidth. The diamond sample itself is heatsunk to a sapphire window, that has a wire loop acting as a microwave antenna glued to it. The fluorescence is collected efficiently by a compound parabolic concentrator [17], and the remaining excitation light is filtered out by a longpass filter. An auto-balanced photodetector [18, 19] collects both the fluorescence as well as a portion of the excitation beam as a reference, cancelling most of the laser intensity noise.

We then use a lock-in modulation scheme at frequencies of  $\omega_{\text{lock}}$  of a few tens of kHz to create the error signals  $S_{+1}$  and  $S_{-1}$  at both transitions. The information gained by monitoring both transitions can then be used to compensate for temperature fluctuations of the sample, which would shift the whole spectrum at once, as shown in Fig. 1 B [20].

To prevent introducing additional noise in later steps, the data is processed on the FPGA of a STEMLab Red-Pitaya, using a modified version of PyRPL [21]. The photodetector output is digitized by one of its fast 14 bit inputs and fed into two lock-in modules. The output of

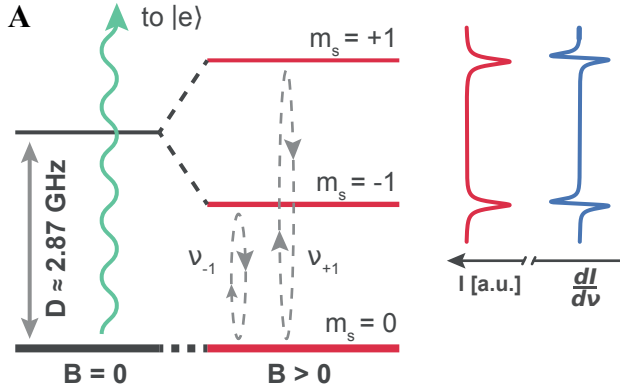


FIG. 2. (A) Simplified  $\text{NV}^-$  center level scheme. The internal spin state can be read out by transferring the system into the excited state - if the centers were in the  $m_s = \pm 1$ , the fluorescence will not be as bright (as indicated by the width of the red lines). Now the Zeeman shift of the  $m_s = \pm 1$  levels can be measured by finding the fluorescence minima. By modulating the microwave frequencies  $\nu_{-1}$  and  $\nu_{+1}$ , a lock in scheme can be employed. (B) Overview of the microwave setup used for performing magnetometry on the NV centers. Everything inside a red box is performed on a RedPitaya's FPGA, with the pale box grouping the lock in functionality.

the lock in modules is then subtracted and sent through both a PI controller and an IIR filter, and the sum of these two signals is outputted to a homebuilt current controller, regulating the current through a small pair of coils.

At the same time, the lock-in modules also modulate the frequencies of arbitrary waveform generators with frequency  $\omega_{\text{lock}}$ . This will later on lead to the modulation visible in the diamond's fluorescence. The arbitrary waveform generators output is mixed with a second AWG, generating sidebands at  $\nu_{\text{HF}} \approx 2.2 \text{ MHz}$  distance, to address all three hyperfine states of the NV centers at the same time. These signals are then outputted on the 14 bit DACs of the RedPitaya.

The outputs are high-pass filtered (allowing us to also

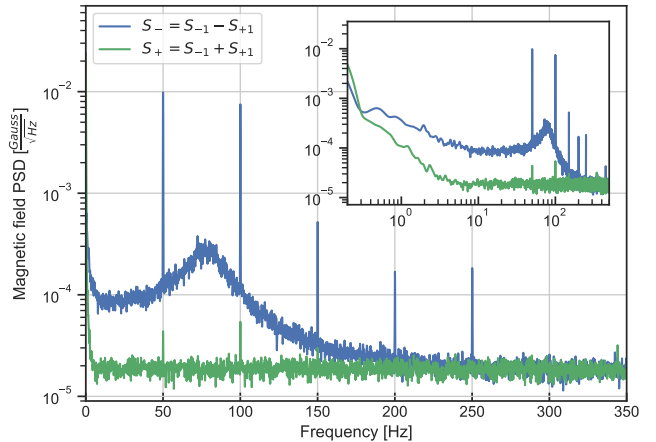


FIG. 3. Sum and difference of the error signals obtained on the two transitions. The inset shows the same data plotted logarithmically, indicating that the temperature noise starts to dominate at low frequencies.

output the current control signal on the same DACs) and then mixed with microwave generators (the two channels of a Windfreaktech SynthHD). These signals are added, amplified (using a MiniCircuits ZHL-16W-43+) and applied to the wire loop around the NV centers. From the fluorescence we can now extract a lock in signal, giving us an error signal proportional to the magnetic field fluctuations in the vicinity of a transition.

The position of these transitions depends on the magnetic field, but also on other factors, most importantly temperature. This effect shifts both transitions equally, so it can be compensated by subtracting the two error signals  $S_{+1}$  and  $S_{-1}$ . Additionally, a signal proportional to the shift of the ZFS  $D$  can be obtained by adding the two signals.

The spectrum of the signals obtained this way are shown in Fig. 3: One can see that the noise at 50 Hz and harmonics (which is magnetic field noise created by the power line) is suppressed in  $S_+$  by a factor 200 for signals far away from the noise floor. From this one can conclude that strong temperature noise is also suppressed by a factor of 200, or 46 dB.

In the inset one can see the same data plotted on a logarithmic frequency scale, which shows that the noise induced by temperature fluctuations starts to become relevant at low frequencies, eventually becoming the dominant source of noise in the individual error signals.

#### IV. MAGNETIC FIELD STABILIZATION

We now employ the magnetic field error signal to cancel out magnetic field fluctuations using a PI controller, also realized on the RedPitaya's FPGA, regulating the current through the small pair of coils. As particularly strong magnetic field noise is present at 50 Hz and harmonics due to power line noise, we implement an IIR

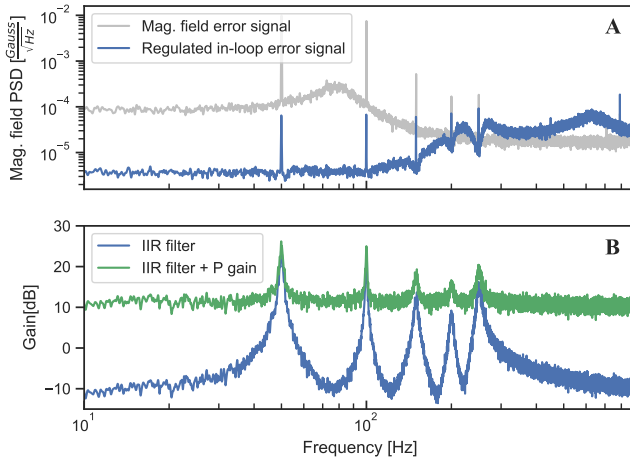


FIG. 4. (A): Magnetic field error signal for an open feedback loop (in grey) and for a closed feedback loop (in blue). (B): The total feedback gain consists of a PI signal (the I part not shown) as well as a IIR filter to increase the noise suppression at 50 Hz and harmonics.

filter to increase the feedback loop gain at those frequencies.

The regulated in-loop error signal as well as the feedback loop's transfer function are shown in Fig. 4. Even though it appears here as if the magnetic field noise is regulated below the sensor's noise floor, this is certainly not the case - the sensor noise has been regulated, and was this way converted to magnetic field noise.

This means, that in order to quantify the magnetic field stability, we need a second, independent sensor. For that we employ a second diamond containing NV centers, using independent optical and microwave setups. In Fig. 1 C one can see a long term measurement performed over 24 hours by monitoring the magnetic field this way. Here, magnetic field noise is suppressed by approximately a factor 5, leaving us with  $123 \mu\text{G}$  of magnetic field noise over a 1 Hz bandwidth. Short term measurements over the whole sensor's bandwidth of 1 kHz yields magnetic field noise of  $1.2 \text{ mG RMS}$ , where the limiting factor is the white noise floor of  $18 \mu\text{G}/\sqrt{\text{Hz}}$  on both sensors, consisting mainly of laser intensity- and microwave noise. This means that increasing the control loop's bandwidth in our case would decrease the magnetic field stability, as no actual magnetic field noise above the sensor noise floor is detectable past a few hundred Hz.

From the obtained measurements in Fig. 1 C we calculate the Allan deviation of the magnetic field stability, as shown in Fig. 5. In addition to the two measurements already discussed, a short term measurement without temperature noise compensation scheme is shown. It clearly indicates the necessity of the temperature noise suppression scheme. The short term measurement with temperature noise compensation drops with the  $\tau^{-1/2}$  scaling expected from white frequency noise. The long term measurements show a broad peak at 60 s. This is noise

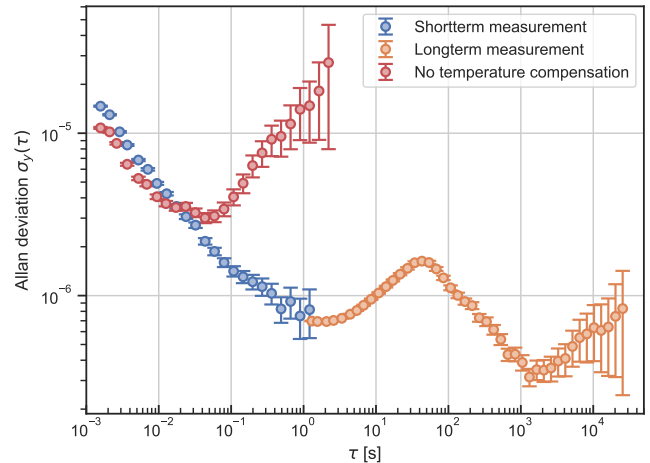


FIG. 5. Allan deviation of the stabilized magnetic field. In addition to the expected improvement with  $1/\sqrt{\tau}$  for white noise on the error signal, a noise peak at  $\tau = 60$  s can be observed, which results from the retuning routine for the microwave generators. The red curve shows the Allan deviation obtained when the magnetic field is only locked to one of the NV center transitions, so without our temperature noise compensation scheme.

created by retuning microwave sources once a minute to follow the temperature shifts of the NV center's transitions. As this time interval can be chosen freely, it can be adjusted to the duty cycle of the experiment, and is not expected to be problematic.

## V. CONCLUSION

In this letter we presented a magnetic field stabilization based on NV centers, with the potential to stabilize magnetic fields much larger than previously possible. In combination with a fiber based approach to reading out the NV's spin states [22, 23], this could allow for a new class of precision experiments in atomic physics.

Large and stable magnetic fields could allow for precision experiments on Feshbach resonances, for instance for the quantum simulation of dipolar droplets [7], or the study of supersolid behaviors at high field values in dipolar quantum gases [24, 25].

Another application would be studying spin changing collisions between bosonic and fermionic species. While, for Bose-Bose mixtures, these resonances typically lie in the range of a few Gauss and have been successfully employed before [5, 26], for the scattering of a bosonic and a fermionic species they occur at much higher field strengths, e.g. for the case of  $^{23}\text{Na}$  and  $^{40}\text{K}$  in the vicinity of 300 G. The magnetic field stabilization demonstrated in this work has the potential to create stable enough magnetic fields in these regimes, and could thus allow for the simulation of quantum electrodynamics [8].

## ACKNOWLEDGMENTS

This work is part of and supported by the DFG Collaborative Research Centre “SFB 1225 (ISOQUANT)”. F. J. acknowledges the DFG support through the

project FOR 2724, the Emmy-Noether grant (project 377616843) and from the Juniorprofessorenprogramm Baden-Württemberg (MWK). D.D. and J.W. acknowledge financial support by the German Science Foundation (DFG) (SPP1601, FOR2724), the EU (ERC) (ASTERIQS, SMel), the Max Planck Society, the Volkswagen Stiftung.

- 
- [1] H. Strobel, W. Muessel, D. Linnemann, T. Zibold, D. B. Hume, L. Pezzè, A. Smerzi, and M. K. Oberthaler, Fisher information and entanglement of non-gaussian spin states, *Science* **345**, 424 (2014).
  - [2] W. Muessel, H. Strobel, D. Linnemann, D. B. Hume, and M. K. Oberthaler, Scalable spin squeezing for quantum-enhanced magnetometry with bose-einstein condensates, *Phys. Rev. Lett.* **113**, 103004 (2014).
  - [3] B. Pasquiou, E. Maréchal, G. Bismut, P. Pedri, L. Vernac, O. Gorceix, and B. Laburthe-Tolra, Spontaneous demagnetization of a dipolar spinor bose gas in an ultralow magnetic field, *Phys. Rev. Lett.* **106**, 255303 (2011).
  - [4] M. Prüfer, P. Kunkel, H. Strobel, S. Lannig, D. Linnemann, C.-M. Schmied, J. Berges, T. Gasenzer, and M. K. Oberthaler, Observation of universal dynamics in a spinor bose gas far from equilibrium, *Nature* **563**, 217 (2018).
  - [5] A. Mil, T. V. Zache, A. Hegde, A. Xia, R. P. Bhatt, M. K. Oberthaler, P. Hauke, J. Berges, and F. Jendrzejewski, A scalable realization of local u(1) gauge invariance in cold atomic mixtures, *Science* **367**, 1128 (2020).
  - [6] P. Ripka, Review of fluxgate sensors, *Sensors and Actuators A: Physical* **33**, 129 (1992).
  - [7] C. R. Cabrera, L. Tanzi, J. Sanz, B. Naylor, P. Thomas, P. Cheiney, and L. Tarruell, Quantum liquid droplets in a mixture of bose-einstein condensates, *Science* **359**, 301 (2018).
  - [8] T. V. Zache, F. Hebenstreit, F. Jendrzejewski, M. K. Oberthaler, J. Berges, and P. Hauke, Quantum simulation of lattice gauge theories using Wilson fermions, *Quantum Science and Technology* **3**, 034010 (2018).
  - [9] F. Baudenbacher, L. Fong de los Santos, J. Holzer, and M. Radparvar, Monolithic low-transition-temperature superconducting magnetometers for high resolution imaging magnetic fields of room temperature samples, *Applied Physics Letters - APPL PHYS LETT* **82** (2003).
  - [10] D. Drung, C. Abmann, J. Beyer, A. Kirste, M. Peters, F. Ruede, and T. Schurig, Highly sensitive and easy-to-use squid sensors, *IEEE Transactions on Applied Superconductivity* **17**, 699 (2007).
  - [11] V. G. Lucivero, P. Anielski, W. Gawlik, and M. W. Mitchell, Shot-noise-limited magnetometer with subpicotesla sensitivity at room temperature, *Review of Scientific Instruments* **85**, 113108 (2014).
  - [12] W. Muessel, H. Strobel, D. Linnemann, D. B. Hume, and M. K. Oberthaler, Scalable spin squeezing for quantum-enhanced magnetometry with bose-einstein condensates, *Phys. Rev. Lett.* **113**, 103004 (2014).
  - [13] T. Wolf, P. Neumann, K. Nakamura, H. Sumiya, T. Ohshima, J. Isoya, and J. Wrachtrup, Subpicotesla diamond magnetometry, *Phys. Rev. X* **5**, 041001 (2015).
  - [14] J. M. Schloss, J. F. Barry, M. J. Turner, and R. L. Walsworth, Simultaneous broadband vector magnetometry using solid-state spins, *Phys. Rev. Applied* **10**, 034044 (2018).
  - [15] S. Steinert, F. Dolde, P. Neumann, A. Aird, B. Naydenov, G. Balasubramanian, F. Jelezko, and J. Wrachtrup, High sensitivity magnetic imaging using an array of spins in diamond, *Review of Scientific Instruments* **81**, 043705 (2010).
  - [16] J. Wrachtrup, C. von Borczyskowski, J. Bernard, M. Orrit, and R. Brown, Optical detection of magnetic resonance in a single molecule, *Nature* **363**, 244 (1993).
  - [17] W. Welford and R. Winston, *The Optics of Nonimaging Concentrators: Light and Solar Energy* (Academic Press, New York, 1978).
  - [18] P. C. D. Hobbs, Noise cancelling circuitry for optical systems with signal dividing and combining means (1992), uS Patent 5,134,276.
  - [19] P. C. D. Hobbs, *Building ElectroOptical Systems: Making it all work* (John Wiley & Sons, Ltd, 2008).
  - [20] V. Ivády, T. Simon, J. R. Maze, I. A. Abrikosov, and A. Gali, Pressure and temperature dependence of the zero-field splitting in the ground state of nv centers in diamond: A first-principles study, *Phys. Rev. B* **90**, 235205 (2014).
  - [21] L. Neuhaus, R. Metzdorff, S. Chua, T. Jacqmin, T. Briant, A. Heidmann, P. . Cohadon, and S. Delglise, Pyrpl (python red pitaya lockbox) an open-source software package for fpga-controlled quantum optics experiments, in *2017 Conference on Lasers and Electro-Optics Europe European Quantum Electronics Conference (CLEO/Europe-EQEC)* (2017) pp. 1–1.
  - [22] S. M. Blakley, I. V. Fedotov, S. Y. Kilin, and A. M. Zheltikov, Room-temperature magnetic gradiometry with fiber-coupled nitrogen-vacancy centers in diamond, *Opt. Lett.* **40**, 3727 (2015).
  - [23] I. V. Fedotov, L. V. Doronina-Amitonova, D. A. Sidorov-Biryukov, N. A. Safronov, S. Blakley, A. O. Levchenko, S. A. Zibrov, A. B. Fedotov, S. Y. Kilin, M. O. Scully, V. L. Velichansky, and A. M. Zheltikov, Fiber-optic magnetic-field imaging, *Opt. Lett.* **39**, 6954 (2014).
  - [24] L. Chomaz, D. Petter, P. Ilzhöfer, G. Natale, A. Trautmann, C. Politi, G. Durastante, R. M. W. van Bijnen, A. Patscheider, M. Sohmen, M. J. Mark, and F. Ferlaino, Long-lived and transient supersolid behaviors in dipolar quantum gases, *Phys. Rev. X* **9**, 021012 (2019).
  - [25] F. Böttcher, J.-N. Schmidt, M. Wenzel, J. Hertkorn, M. Guo, T. Langen, and T. Pfau, Transient supersolid properties in an array of dipolar quantum droplets, *Phys. Rev. X* **9**, 011051 (2019).
  - [26] X. Li, B. Zhu, X. He, F. Wang, M. Guo, Z.-F. Xu, S. Zhang, and D. Wang, Coherent heteronuclear spin dy-

namics in an ultracold spinor mixture, Phys. Rev. Lett. **114**, 255301 (2015).